

RAPID COMMUNICATION

# Smart construction of three-dimensional hierarchical tubular transition metal oxide core/shell heterostructures with high-capacity and long-cycle-life lithium storage <sup>☆</sup>



Jiexi Wang<sup>a,1</sup>, Qiaobao Zhang<sup>b,1</sup>, Xinhai Li<sup>a</sup>, Bao Zhang<sup>a,\*</sup>,  
Liqiang Mai<sup>c,\*</sup>, Kaili Zhang<sup>b,\*</sup>

<sup>a</sup>School of Metallurgy and Environment, Central South University, 932, South Lushan Road, Changsha, P.R. China, 410083

<sup>b</sup>Department of Mechanical and Biomedical Engineering, City University of Hong Kong, 83 Tat Chee Avenue, Hong Kong

<sup>c</sup>State Key Laboratory of Advanced Technology for Materials Synthesis and Processing, WUT-Harvard Joint Nano Key Laboratory, Wuhan University of Technology, Wuhan, 430070, P.R. China

Received 4 November 2014; received in revised form 30 December 2014; accepted 1 January 2015  
Available online 9 January 2015

## KEYWORDS

Transition metal oxide;  
Nanomaterial;  
Tubular structure;  
Anode;  
Lithium ion battery

## Abstract

In order to realize new high performance electrodes for lithium-ion batteries (LIBs), the careful design of nanoarchitectures and effective hybridization of active materials are research areas of great interest. Here, we present a simple and highly controllable two-step fabrication technique, followed by a heat treatment process, for the large-scale in situ growth of 3D hierarchical tubular CuO/other metal oxides core/shell heterostructure arrays that are directly grown on Cu foam. As a proof-of-concept demonstration of the application of such 3D hierarchical tubular heterostructure arrays, the prepared tubular CuO/CoO core/shell arrays are investigated as binder- and conductive agent-free anodes for LIBs, exhibiting an impressive capacity of 1364 mAh g<sup>-1</sup> at a current density of 100 mA g<sup>-1</sup> after 50 cycles and maintaining 1140 mAh g<sup>-1</sup> after 1000 cycles at 1.0 A g<sup>-1</sup>. This excellent electrochemical performance can be attributed to the unique hollow porous architecture consisting of 3D hierarchical tubular core/shell architectures, and the effective hybridization of two electrochemically cohesive

<sup>☆</sup>Supporting Information is available

\*Corresponding authors.

E-mail addresses: [xinhaili\\_csu@126.com](mailto:xinhaili_csu@126.com),  
[csuzb@vip.163.com](mailto:csuzb@vip.163.com) (B. Zhang), [mlq518@whut.edu.cn](mailto:mlq518@whut.edu.cn) (L. Mai),  
[kaizhang@cityu.edu.hk](mailto:kaizhang@cityu.edu.hk) (K. Zhang).

<sup>1</sup>These authors contributed equally to this work.

active materials. Our work shows that this material has great potential for high-energy and high-power energy storage applications.

© 2015 Elsevier Ltd. All rights reserved.

## Introduction

Lithium ion batteries (LIBs) are one of the most promising types of energy storage devices and have been the focus of tremendous amounts of interest. [1-8] Nanostructured transition metal oxides (TMOs) have long been focused on as potential anode materials for LIBs, given their ease of large-scale fabrication and high theoretical capacity. [2,6,9-20] Generally, it is not suitable to use TMOs as cathode due to their too low potential (only about 1 V vs.  $\text{Li}^+/\text{Li}$ ). Moreover, except for lithium metal, it is difficult to find a kind of Li-supplied material that owns low enough potential to match TMOs. Though owning relatively high potential, TMOs normally own 2-3 times higher specific capacity than commonly used graphite, making such kind of materials a potential anode to substitute graphite to obtain higher energy density, especially in high-voltage cells. However, due to some problematic intrinsic properties, including low electrical conductivity, slow lithium ion diffusion rate and associated parasitic side reactions, LIBs solely using single-phase nanostructured metal oxides for electrodes often suffer from low capacity and poor capacity retention over extended cycling, leading to a less satisfactory battery life relative to the commercial standard. [2,17,21] To address these drawbacks and boost electrochemical performance, one promising solution involves the use of integrated array architectures involving hierarchical porous nanostructures, consisting of a combination of two types of materials that are connected on conductive substrates. [2,22-25] These materials can be directly employed as binder- and conductive agent-free electrodes for LIBs and have several apparent advantages, including large active surface area, short diffusion path lengths for electrons and ions, and the potential presence of a synergistic effect from the two nanostructure materials, which add up to an enhanced electrochemical performance for LIBs. [2,22] In particular, with a large surface area and direct electronic/ionic transport pathways, hierarchical three-dimensional (3D) branched core-shell nanowire heterostructures grown directly on a conductive substrate have been shown to be well-suited designs for high-performance LIBs. [2,22,23,26-33] Despite these advances, the development of a simple, broadly applicable and controlled procedure for effectively synthesizing self-supported, transition-metal oxide core/shell nanosized array heterostructures on conductive substrates, especially with hierarchical porous tubular architectures has been highly desirable but still very challenging. Here, for the first time, we present a facile, controllable and effective approach, namely solution immersion and chemical bath deposition (CBD) followed by calcination, to produce hierarchical porous 3D core/shell arrays with tubular heterostructures on copper foam. The heterostructures are composed of CuO nanotubes as the

backbone together with various branched nanostructured metal oxides, including CoO,  $\text{NiCo}_2\text{O}_4$ ,  $\text{ZnCo}_2\text{O}_4$  and  $\text{Cu}_x\text{Co}_{3-x}\text{O}_4$ . The growth mechanism of the in-situ formation of tubular CuO cores together with branched nanostructured metal oxides shells is systemically investigated. These nanostructured branched metal oxides facilitate charge transfer, and the porous structure and high surface area of this design, which results in large reactive sites, is beneficial for the electrochemical reaction at the interface of the electrode and electrolyte. [19,22,23] In addition, this architecture's tubular structure makes it possible for the electrode to withstand large volume changes during repeated charge-discharge cycles, which may lead to an improved long term cycle performance and a high rate capability. [19,23,30,34] As an example of the functional properties of these 3D core/shell arrays with tubular heterostructures, the as-prepared tubular CuO/CoO core/shell arrays are expected to demonstrate an enhanced electrochemical performance with high lithium storage capacity and excellent cycling stability when investigated as binder- and conductive agent-free electrodes for LIBs.

## Experimental section

### Synthesis of $\text{Cu}(\text{OH})_2$ nanorods on copper foam

Commercially available copper foam from Changsha Lyrun New Materials Co. Ltd. with a thickness of 0.5 mm and dimensions of  $7.0 \times 7.0$  cm was used as a conductive substrate. The copper foam was ultrasonically cleaned in ethanol for 10 min, adequately rinsed with ethanol and distilled water, and blow-dried with compressed air. The cleaned copper foam was then immersed in an aqueous solution of  $2.5 \text{ mol} \cdot \text{L}^{-1}$  sodium hydroxide and  $0.1 \text{ mol} \cdot \text{L}^{-1}$  ammonium persulphate at room temperature for about 20 min. Following this, the copper foam was taken out of the solution and rinsed with de-ionized water, then dried with nitrogen.

### Synthesis of 3D hierarchical tubular and solid CuO/CoO core/shell heterostructure arrays

To create a typical set of samples, 3.16 g of cobalt(II) sulfate heptahydrate (0.075 M) and 10.22 g of urea (1.125 M) were dissolved in 150 mL of distilled water in a 250 mL Pyrex beaker and stirred to form a clear pink solution. The previously prepared copper foam with Cu(OH)<sub>2</sub> nanorod arrays, 4.5 cm (width)  $\times$  6.8 cm (length) in size and with the backside coated with polyimide tape, were immersed in the mixture, which was then sealed with aluminum foil, maintained at 85 °C for 0.5 h to 4 h, and cooled to room temperature. The substrates were then taken out of the solution, rinsed with distilled water, and

ultrasonically cleaned in alcohol. Finally, the samples were annealed at 350 °C in argon for 2 h in order to prepare the hierarchical CuO/CoO core/shell heterostructure arrays. For comparison, CoO nanostructures grown directly on copper foam (CBD-CoO) were synthesized under the same conditions.

To obtain solid CuO/CoO core/shell nanorod heterostructure arrays on Cu foam, CuO nanorods rather than Cu(OH)<sub>2</sub> nanorods on Cu foam were used. The same process for integrating CoO with CuO nanorods by CBD followed by calcination was applied. Details can be found in ESI-1.

## Sample characterization

The morphology, crystalline structure and composition of as-grown CuO nanorods, CoO nanostructures and hierarchical solid and tubular CuO/CoO core/shell heterostructure arrays were characterized with field-emission scanning electron microscopy (SEM, Hitachi S4800), transmission electron microscopy (TEM, Titan G2 60-300 with image corrector) and X-ray diffraction (XRD, Rigaku SmartLab). The elemental valence states of the prepared samples were determined with an X-ray photoelectron spectrometer (XPS, Kratos Model XSAM800) equipped with a Mg K<sub>α</sub> achromatic X-ray source (1235.6 eV).

## Electrochemical properties evaluations

In order to investigate electrochemical performance, the synthesized hierarchical tubular CuO/CoO core/shell heterostructure arrays grown directly on copper foam substrate were dried in vacuum for 12 h at 120 °C, and punched to form 12 mm diameter disks, used as working electrodes. The methodological details for determining the mass loading on the electrodes are available in ESI-2, and the amount of the active material on the tubular CuO/CoO nanowire electrode is 2.95 mg. Lithium foil was used as the counter and reference electrodes, and the CR2025 half cells were assembled in a dry Ar-filled glove box using a polypropylene micro-porous film as a separator and 1 M LiPF<sub>6</sub> in EC/DMC/EMC (1:1:1, in volume) as electrolyte. The electrochemical performance of cells was evaluated by charging and discharging over a voltage range of 3 V to 0.01 V vs. Li/Li<sup>+</sup> at room temperature with a Land BT-10 Tester (Wuhan, China). Cyclic voltammetry (CV) and electrochemical impedance spectroscopy (EIS) measurements were conducted with an electrochemical work station (CHI660A) with a three-electrode system incorporating tubular CuO/CoO core/shell heterostructure arrays as the working electrode and Li foil as the counter and reference electrodes. The CV tests were performed at a scanning rate of 0.1 mV s<sup>-1</sup>. The impedance spectra were recorded using an AC voltage of 5 mV and a working frequency range of 10<sup>-2</sup> Hz to 10<sup>5</sup> Hz.

## Results and discussion

### Structure characterization and growth mechanism

As illustrated in Fig. 1, first, high density Cu(OH)<sub>2</sub> nanorod arrays are prepared in large scale on copper foam through

the solution immersion method under ambient conditions (Fig. 1a, b), in order to serve as the backbone for the later growth of CoO nanosheets. Subsequently, branched cobalt precursor (cobalt hydroxide carbonate) nanosheets are grown uniformly on the Cu(OH)<sub>2</sub> nanorod backbones by the CBD method (Fig. 1c), forming the 3D hierarchical tubular Cu(OH)<sub>2</sub>/Co precursor core/shell heterostructure arrays. Finally, these as-obtained 3D hierarchical tubular Cu(OH)<sub>2</sub>/Co precursor core/shell heterostructure arrays are converted to 3D hierarchical tubular CuO/CoO core/shell heterostructure arrays through calcination (Fig. 1d). Alternatively, to achieve the creation of solid CuO/CoO core/shell heterostructure arrays on Cu foam, Cu(OH)<sub>2</sub> nanorods on Cu foam are first thermally converted to CuO nanorods in argon gas before undergoing the CBD process, as illustrated in Fig. S1.

The morphological and structural analyses of as-prepared Cu(OH)<sub>2</sub> nanorods in Fig. S2 reveal a high density of single-crystal Cu(OH)<sub>2</sub> nanorods vertically grown on the surface of the copper foam with large scale uniformity. The CuO nanorod arrays could be easily obtained with a simple thermal conversion of the corresponding precursor of Cu(OH)<sub>2</sub> nanorods with well-maintained morphologies under flowing high-purity argon gas (Fig. S3). XRD and XPS results of final sample demonstrate successful fabrication of CuO/CoO heterostructures on Cu foam (Fig. S4). After the deposition of CoO, as shown in Fig. 2a-b, the uniformity of the array structure is retained well and numerous ultrathin branched CoO nanosheets are newly decorated on the surface of the CuO nanotubes. A magnified SEM image shown in the inset of Fig. 2b unambiguously reveals that the CoO branches are fully coated onto the CuO nanotube core with a good uniformity in size and a fairly homogenous distribution along the nanorod, forming 3D core/shell architecture with a large scale, highly open structure. This in turn indicates that the interface contact between CuO nanotube cores and branched CoO nanosheet shells is excellent, which could play an important role in improving the electrochemical performance of the material. Moreover, the diameter, length, and density of the secondary CoO branches can be tailored to demand by changing the chemical reaction time (Fig. S5). Compared to solid CuO/CoO nanorod arrays (Fig. S6), the as-fabricated tubular CuO/CoO heterostructure on Cu foam has a more uniform distribution and does not contain solid bulk particles. As shown in Fig. 2c, the hollow interior of CuO can be clearly observed, with numerous, highly uniform and tiny CoO nanosheets closely attached on the surface of the CuO nanotubes. These CoO nanosheet shells, with a thickness of about 200 nm, are highly porous with pores ranging from 2 to 5 nm in size and themselves made up of numerous interconnected nanocrystallites with sizes of 2-10 nm, as seen in Fig. 2d. HRTEM image (Fig. 2e) of CoO nanosheet shells shows clear lattice fringes with a measured interplanar spacing of 0.24 nm and 0.20 nm, corresponding to the interplanar distances of the (1 1 1) and (2 0 0) planes of cubic CoO, respectively. [35] The nitrogen isothermal adsorption-desorption measurement (Fig. S7) reveals mesoporous features of CoO nanosheet shells in the narrow pore region of 20-40 nm with a specific surface of 40.2 m<sup>2</sup> g<sup>-1</sup>. This 3D hierarchical tubular core/shell structure analysis is supported by TEM elemental mapping as shown in Fig. 2f.

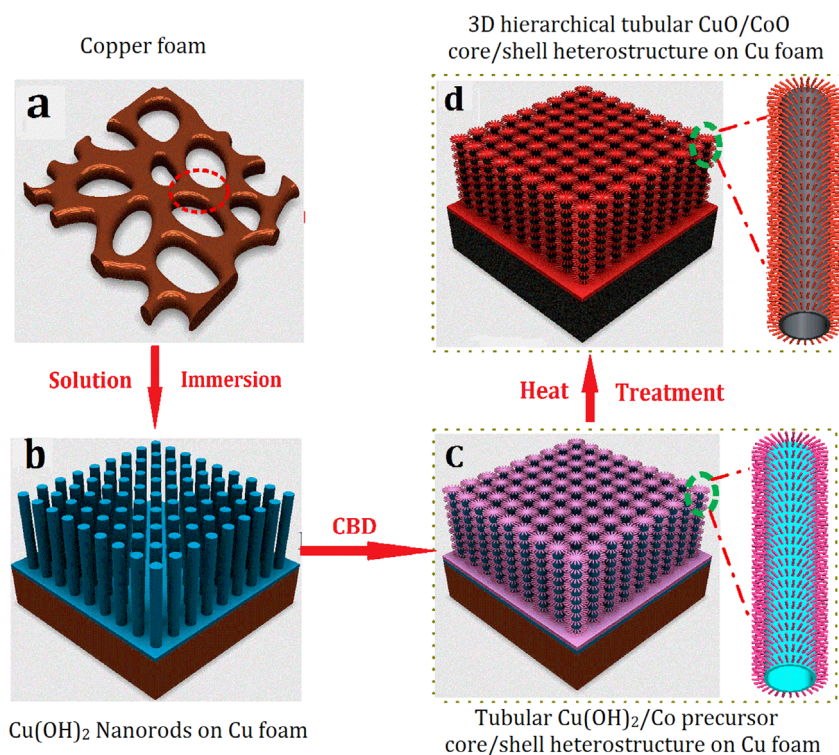


Fig. 1 Fabrication process of 3D hierarchical tubular CuO/CoO core/shell heterostructure arrays on Cu foam.

It is observed that the signals from Co and O are strongly detected in the backbone and branch region, while the Cu signals are detected solely in the backbone region. A hollow interior can be clearly observed in the backbone region from Fig. 3d, suggesting the tubular structure of the CuO cores. These results indicate that branched CoO nanosheet shells are successfully synthesized on the surface of hollow CuO cores, forming a hierarchical tubular CuO/CoO core/shell configuration. However, the sample prepared by using CuO nanorods rather than Cu(OH)<sub>2</sub> nanorods on Cu foam substrate displays a solid CuO backbone (i.e., lacking a tubular structure) together with CoO nanosheet branches (Fig. S8). The hierarchical tubular CuO/CoO core/shell heterostructure resulting from this procedure can also be produced on Cu mesh with no apparent difference in the morphology, as shown in Fig. S9. Remarkably, the simple yet powerful CBD/calcination method can also be readily extended to grow a variety of other metal oxides, including Co<sub>3</sub>O<sub>4</sub>, NiCo<sub>2</sub>O<sub>4</sub>, ZnCo<sub>2</sub>O<sub>4</sub> and Cu<sub>x</sub>Co<sub>3-x</sub>O<sub>4</sub>, on the surfaces of CuO nanotube arrays that have been developed directly on Cu foam (Fig. S10) as well as on other nanostructures on conductive substrates. These include NiSi<sub>x</sub> on Ni foam, CuO nanowires on Ni foam, CuO microflowers on Cu foam and flexible carbon cotton (Fig. S11), demonstrating the high efficiency and broad applications of this synthesis strategy.

To understand the formation of both the hierarchical tubular and solid CuO/CoO core/shell heterostructures, Cu(OH)<sub>2</sub> nanorods as well as CuO nanorods formed from the thermal conversion of Cu(OH)<sub>2</sub> nanorods, grown directly on Cu foam, are used for subsequent growth of CoO. Fig. 3 illustrates the formation process of tubular (route 1) and solid (route 2) CuO/CoO core/shell heterostructures. The TEM image shown in Fig. 3b unambiguously reveals that the interior of the final Cu(OH)<sub>2</sub>/Co-precursor nanostructure is

hollow in the CBD process, while the interior of the final CuO/Co-precursor nanostructure is solid (Fig. 3e), which can also be observed clearly in TEM images shown in Figure S12. This suggests that the hierarchical tubular structure is indeed formed in the CBD process by using Cu(OH)<sub>2</sub> nanorods on Cu foam as substrate. After calcination, the hierarchical tubular or solid structure of CuO/CoO is well maintained, as depicted in Fig. 3c and Fig. 3f as well as the STEM results in Fig. S13(a, b) and (c, d), respectively. To verify the role of urea on the formation of the tubular structure, the as-obtained Cu(OH)<sub>2</sub> nanorods on Cu foam are reacted with a urea-only control solution in the same CBD process under the same conditions. Almost no obvious morphological or crystallinity changes in the Cu(OH)<sub>2</sub> nanorods are found (Fig. S14), suggesting that the control solution has no significant effect on the formation of tubular-structured Cu(OH)<sub>2</sub>.

The formation of the tubular structure can be understood with help from Fig. 3. First, NH<sub>3</sub> and CO<sub>2</sub> are released by the decomposition of urea at 85°C, by Eq. (1). Next, NH<sub>4</sub><sup>+</sup>, OH<sup>-</sup> and H<sup>+</sup>, CO<sub>3</sub><sup>2-</sup> are formed by the slow hydrolyzation of NH<sub>3</sub> and CO<sub>2</sub> in solution, respectively, based on Eqs. (2) and (3). Afterwards, the cobalt precursor (cobalt hydroxide carbonate) is obtained through the reaction of Co<sup>2+</sup> with OH<sup>-</sup> and CO<sub>3</sub><sup>2-</sup> (Eq. (4)), leaving an increased concentration of NH<sub>4</sub><sup>+</sup> and H<sup>+</sup> in solution and thus generating a weak acidic environment. [36] Due to the solubility difference between CuO and Cu(OH)<sub>2</sub> in a NH<sub>3</sub>-NH<sub>4</sub><sup>+</sup>-H<sub>2</sub>O leaching system, the NH<sub>4</sub><sup>+</sup> (H<sup>+</sup>) ions can only react with Cu(OH)<sub>2</sub> (Eqs. (5) and (6)). As a result, the inner Cu(OH)<sub>2</sub> core in “route 1” is slowly dissolved, forming tubular structure, while the inner CuO core in “route 2” remains unchanged. Meanwhile, the in-situ formed cobalt hydroxide carbonate would spontaneously and preferentially attach to the Cu(OH)<sub>2</sub> surface, forming active

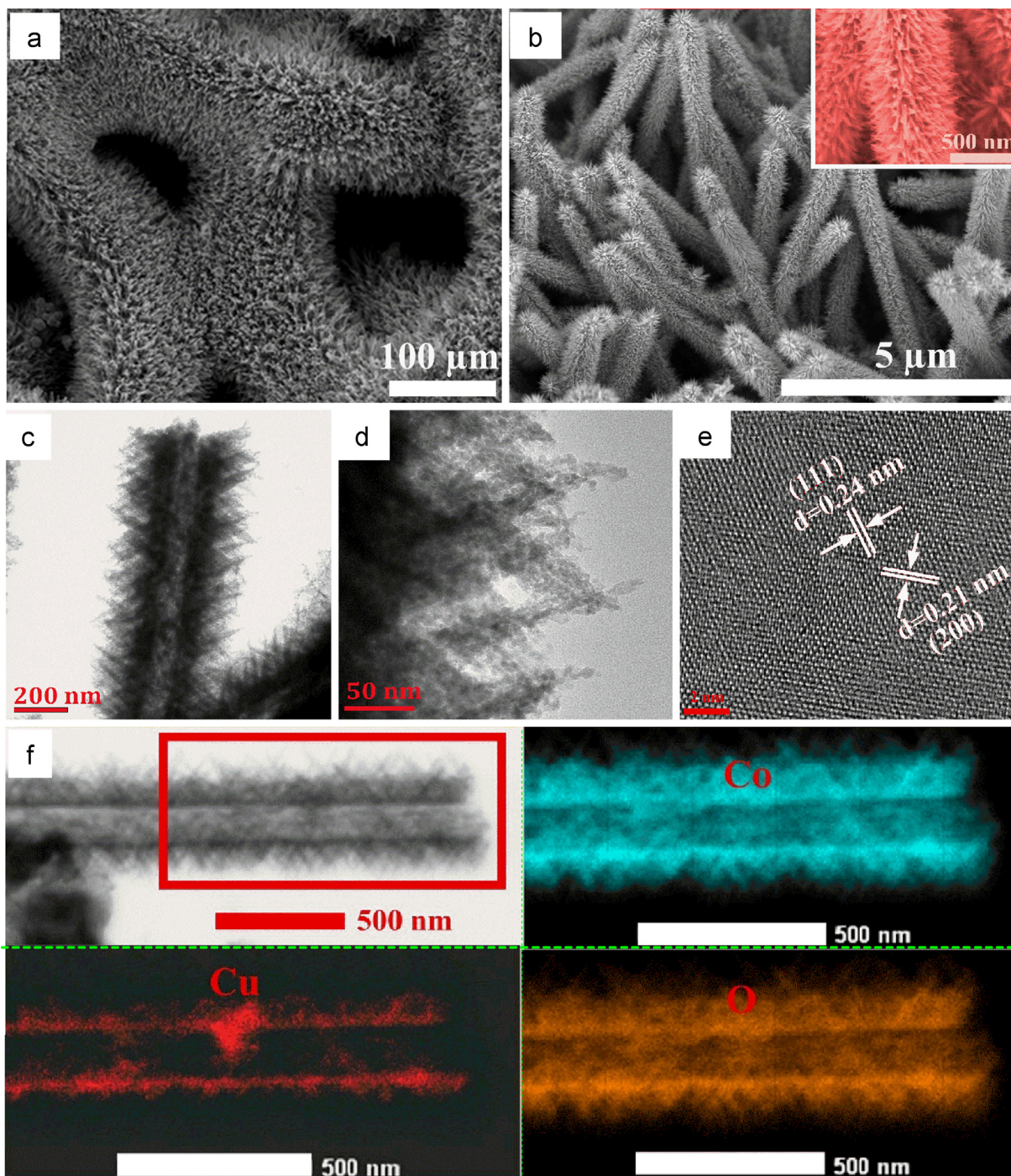


**Fig. 2** (a) low-magnification and (b) high-magnification SEM images, (c, d) TEM and (e) HRTEM images of hierarchical tubular CuO/CoO core/shell heterostructure; (f) EDS mapping results of a single hierarchical tubular CuO/CoO core/shell heterostructure.

nucleation centers by reducing the surface energy. As the reaction proceeds, the inner  $\text{Cu}(\text{OH})_2$  nanorod cores are gradually consumed, while the newly produced cobalt hydroxide carbonate seed nanoparticles continuously nucleate, self-assemble and crystallize along the active nucleation sites through an oriented growth process, forming the final cobalt carbonate hydroxide nanosheets on the surface of  $\text{Cu}(\text{OH})_2$  nanorod cores and resulting in the 3D hierarchical tubular CuO/CoO core/shell heterostructure after heat treatment. To further confirm this explanation, CuO nanowires on Ni

foam synthesized by the oxidation of e-beam Cu film as substrate are also used to prepare a sample with CuO/ $\text{Co}_3\text{O}_4$  core/shell heterostructure through an identical CBD process followed by heat treatment in air, and the TEM images (Fig. S15) clearly reveal that the nanowire structure of CuO is well maintained and the  $\text{Co}_3\text{O}_4$  nanosheets are uniformly and densely attached to the CuO surface. This confirms that Cu(OH)<sub>2</sub> is more easily etched than CuO in such a CBD process and thus predisposes to form the observed hierarchical tubular CuO/CoO core/shell heterostructure.

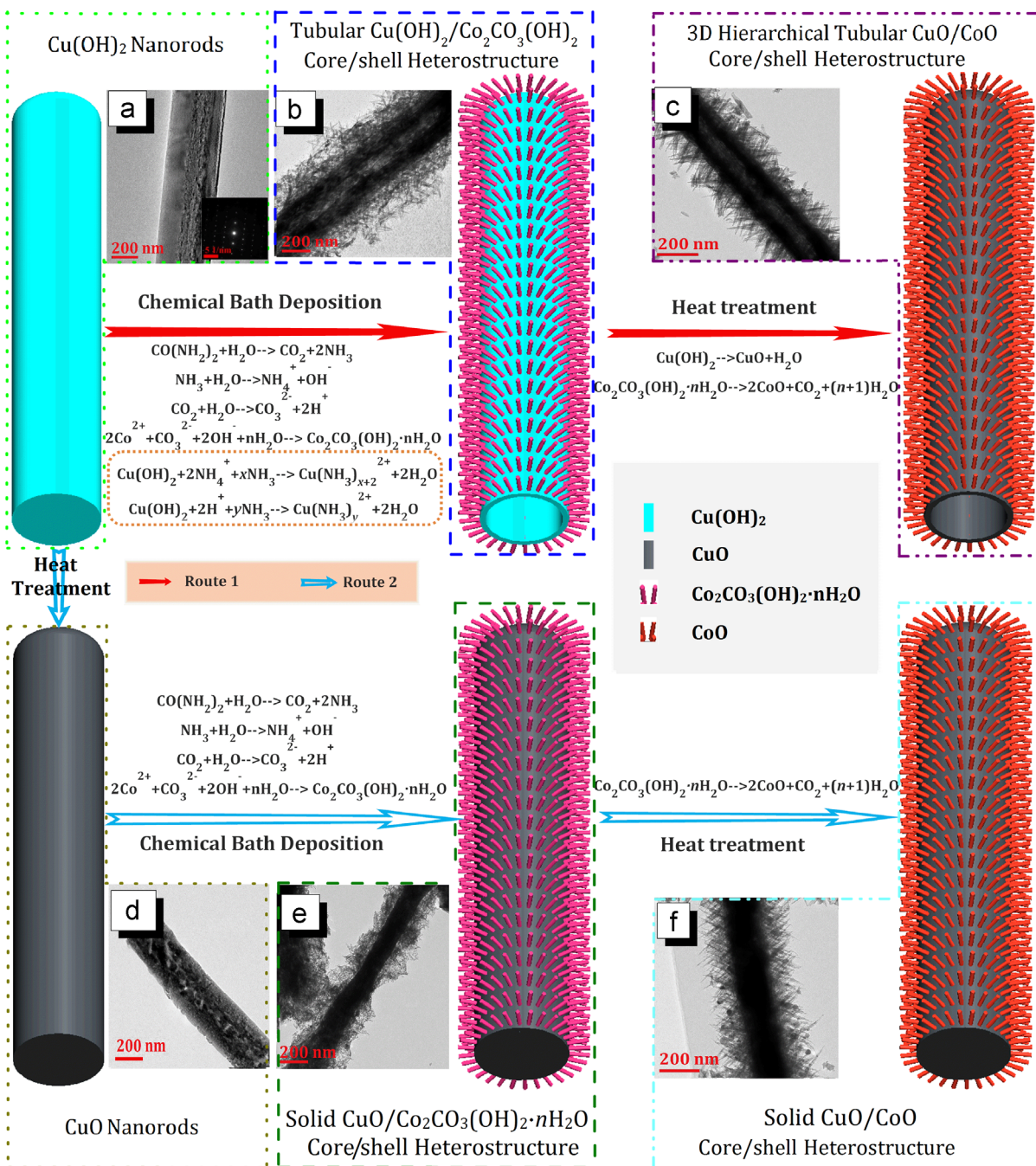
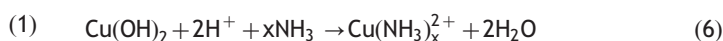
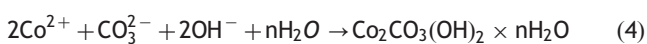
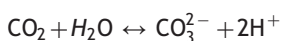


**Fig. 3** schematic diagram to illustrate the formation mechanisms of hierarchical tubular (route 1) and solid (route 2) CuO/CoO core/shell heterostructures.



### Application as lithium ion battery anode

Fig. 4a displays the representative CV curves of tubular CuO/CoO core/shell arrays used as an anode, where the characteristic redox peaks of CuO [Fig. S16(a)] and CoO [Fig. S16(b)] can be observed. [37,38] The corresponding peaks show no significant shift since 2<sup>nd</sup> cycle, indicating a good reproducibility

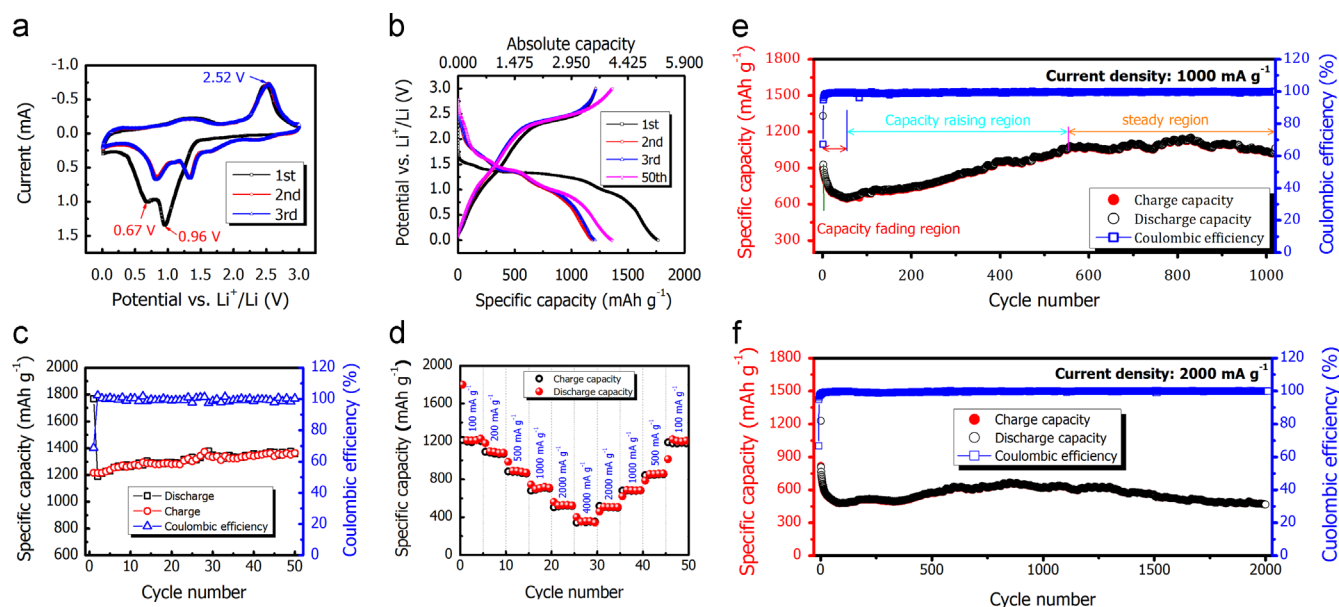


**Fig. 4** Electrochemical performance of as-fabricated tubular CuO/CoO core/shell array anode on copper foam: (a) CV curves at the scan rate of  $0.1 \text{ mV s}^{-1}$  and the voltage range of 3.0-0.01 V, (b) discharge-charge profiles and (c) cycling performance between 3.0 and 0.01 V at  $100 \text{ mA g}^{-1}$ , (d) rate capability in the current range of 100-4000  $\text{mA g}^{-1}$ , (e) long-term cycle performance at  $1.0 \text{ A g}^{-1}$ , and (f) long-term cycle performance at  $2.0 \text{ A g}^{-1}$ .

and high reversibility of the redox reaction. The Discharge-charge profiles of the prepared tubular CuO/CoO core/shell heterostructure array anode as shown in Fig. 4b compare well with the shape of CV curves. The anode delivers an initial reversible charge capacity of  $1216 \text{ mAh g}^{-1}$  with a coulombic coefficient of 69%. The initial irreversible capacity loss of the composite electrode can be ascribed to SEI film formation and electrolyte decomposition. [26] In the subsequent cycle, the coulombic efficiency of the prepared tubular CuO/CoO core/shell heterostructure array electrode increases to more than 98% (Fig. 4c), indicating a high discharge-charge reversibility. As seen in Fig. 4c, the prepared tubular core/shell nano hybrid shows a charge capacity increasing from  $1216$  to  $1364 \text{ mAh g}^{-1}$  over 50 cycles. This feature of capacity increase upon cycling may be related to the continuous formation of a polymeric gel layer on the surface of nano-sized metal oxides that has the ability of  $\text{Li}^+$  storage. [39-45] Another reason for the anomalous capacity of nano-sized metal oxides is proposed to be associated with the formation of oxygen-rich layer on the surface. [46] The electrochemical performance of the prepared composite anode is excellent when compared to both CuO nanorods [Fig. S16(c, e)] and CoO nanoneedles [Fig. S16(d, f)] on Cu foam.

Furthermore, the tubular CuO/CoO core/shell composite electrode also exhibits an excellent rate capability and reversibility as well as long-term cycle performance. As shown in Fig. 4d, the first-cycle charge capacities of the composite electrode are  $1218$ ,  $1019$ ,  $883$ ,  $681$ ,  $505$ , and  $342 \text{ mAh g}^{-1}$  at the current densities of  $100$ ,  $200$ ,  $500$ ,  $1000$ ,  $2000$ , and  $4000 \text{ mA g}^{-1}$ , respectively. When the high current density is reduced back to a low current density, the original high charge capacity is regained. The long term cycle performances of tubular CuO/CoO core/shell array anodes are shown in Fig. 4e and f, and are obtained by directly applying high currents of  $1.0$  and  $2.0 \text{ A g}^{-1}$  respectively to the cells, without activation through low current. It can be clearly seen in Fig. 4e that the

trend of capacity as a function of cycle number displays three stages, including a rapid fading capacity region covering the first 55 cycles (from  $895$  to  $644 \text{ mAh g}^{-1}$ ), then a capacity raising region in the subsequent 500 cycles (from  $644$  to  $1078 \text{ mAh g}^{-1}$ ) and finally a region of relatively steady capacity. The quick capacity fading during the first few tens of cycles may be attributed to structural degradation and reorganization, [47,48] and could be avoided through activation with a low current (Fig. S17). The rising capacity in the second region is likely due to a possible activation process, which is commonly observed in various nanostructured metal oxide electrodes. [40-42,44] This rise in capacity is further elucidated by the capacity plateaus changes shown in Fig. S18. It is observed that part of the contribution to the capacity increase occurs at low voltage (below  $0.8 \text{ V}$ ). This phenomenon may attributed to the reversible formation and decomposition of an organic polymeric-gel-like film caused by kinetically activated electrolyte degradation, which could act as reservoirs for storage of excess  $\text{Li}^+$  ions through a so-called “pseudo-capacitance-type behavior”. [40,47,49-50] After that, the capacity tends toward a steady equilibrium, maintaining about  $1050$ - $1140 \text{ mAh g}^{-1}$  for a large number of cycles, which is higher than the reported results of other metal oxides nanocomposite anodes as shown in Table S1 in supporting information. Even cycled at  $2000 \text{ mA g}^{-1}$  for 2000 cycles (Fig. 4f), the cell can maintain a high capacity of  $466 \text{ mAh g}^{-1}$ , which is superior to the theoretical capacity of graphite ( $374 \text{ mAh g}^{-1}$ ). This high capacity retention at such elevated current densities indicates that the tubular CuO/CoO core/shell array anode possesses excellent cycle performance.

The superior electrochemical performance of the fabricated tubular CuO/CoO core/shell array anodes can be attributed to the well-designed hierarchical tubular structure and synergistic effects of the hollow CuO nanotube backbone combined with branched CoO nanosheet shells, and can be understood from the following considerations. Firstly, as shown in Fig. 5,

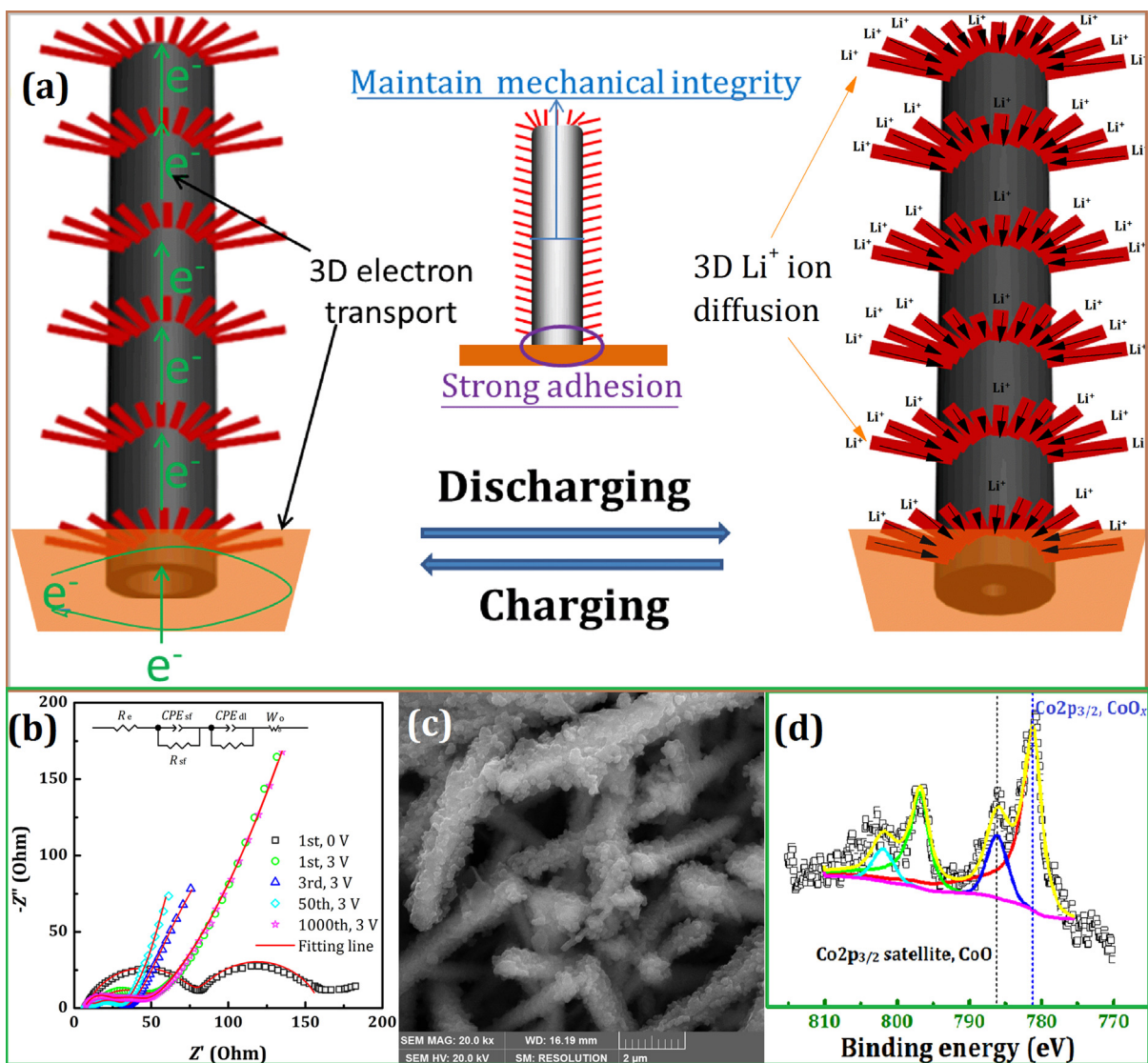


**Fig. 5** (a) Pathways for  $e^-$  conduction and lithium ion diffusion during electrochemical reaction process in tubular CuO/CoO core/shell heterostructure on Cu foam; (b) Nyquist plots of as-fabricated cell composed of tubular CuO/CoO core/shell heterostructure at different state; (c) SEM image and (d) XPS Co 2P curve of as-fabricated tubular CuO/CoO core/shell heterostructure after 50 cycles.

the highly ordered 1D geometry of the tubular CuO backbone is electrically connected to the current collector (3D porous Cu foam) in a way that can provide short and straight electron pathways, allowing for efficient electron transport in the electrode as well as reducing the resistance for electron injection from the current collector to the electrode, which leads to fast charge/discharge capabilities. [27,28] As a result, the cells own small charge transfer resistance as shown in Fig. 5b. Secondly, the hierarchical tubular structure's exterior construction by numerous mesoporous nanosheets facilitates electrolyte penetration into the inner regions of the CuO nanotube cores as well as the rest of the composite, which enables a sufficient electrode-electrolyte contact area to give rise to a high  $\text{Li}^+$  ion flux across the interface and thus account for the high reversible capacity and good rate capability observed. [23] It can be confirmed by very small surface-film impedance as demonstrated in Table S2. The highly porous CoO nanosheets are composed of many small nanoparticles, which yield plentiful active sites for the insertion of Li ions and

enough void spaces to act as a buffer against volume change as well as to shorten diffusion paths for electrons/Li ions, giving rise to high capacities. [49,51-53] SEM (Fig. 5c), and XPS (Fig. 5d) results accompanied with TEM (Fig. S19a-b) and STEM (Fig. S19c-d) analyses of the cycled electrode demonstrate that the fabricated tubular sample maintains the original structure, morphology and composition distribution, further proving the structural stability of this smart construction during repeated discharge-charge process. Meanwhile, the hollow CuO cores are connected to Cu foam with strong adhesion and are able to maintain mechanical integrity, so that it acts to effectively accommodate strain, which can allow the nanotubes to increase in diameter and length without breaking, thereby enhancing the cycle stability. [54] Thirdly, the open space between tubular CuO/CoO core/shell array provides a larger reaction surface area and allows for the diffusion of the electrolyte into the inner region of the electrodes, a behavior beneficial for the full utilization of active materials. [23] The amount of free space also helps to

efficiently accommodate the large volume changes induced by lithium insertion/extraction, leading to excellent cycle performance. Finally, the synergistic contributions from the porous ultrathin CoO shells and tubular CuO cores is also partially responsible for the observed high capacities, outstanding cycling performance and rate capacities.

## Conclusions

In summary, the fabrication of novel, 3D, tubular and solid CuO/CoO core/shell heterostructure arrays grown directly on copper foam has been demonstrated by means of a simple, broadly applicable and high-efficiency two-step solution process followed by heat treatment. The obtained tubular CuO/CoO core/shell heterostructure arrays on copper foam are used as binder- and conductive-agent-free electrodes for LIBs, performing excellently and exhibiting high capacity, desirable rate capability and outstanding cycling stability in comparison to either of the material's individual components. As a result of the material's advantageous structural features and synergetic hybridization of two carefully tailored active materials, tubular CuO and highly porous CoO nanosheets, the tubular CuO/CoO core/shell heterostructure arrays are a promising avenue of exploration for high-performance LIBs. Such a hollow core/shell nanostructure could represent an effective way to realize high-performance electrode materials based on metal oxides for LIBs and may also possess great application potential in other fields such as supercapacitors.

## Acknowledgment

This work was financially supported by the National Basic Research Program of China (973 Program, Grant No. 2014CB643406), the City University of Hong Kong (Grant No. 9667100), the Fundamental Research Funds for the Central Universities of Central South University (Grant No. 2014zzts026), and the Principal Scholarship for Top Creative PhD Candidates. We also thank the Advanced Research Center of CSU for performing HRTEM examination and EDS elemental mapping.

## Appendix A. Supporting information

Supplementary data associated with this article can be found in the online version at <http://dx.doi.org/10.1016/j.nanoen.2015.01.003>.

## References

- [1] L. Ji, Z. Lin, M. Alcoutlabi, X. Zhang, *Energy Environ. Sci.* 4 (2011) 2682-2699.
- [2] J. Jiang, Y. Li, J. Liu, X. Huang, C. Yuan, X. Lou, *Adv. Mater.* 34 (2012) 5166-5180.
- [3] J. Bruce, P.G. Scrosati, B. Tarascon, *Angew. Chem. Int. Ed.* 47 (2008) 2930-2946.
- [4] B. Dunn, H. Kamath, J.-M. Tarascon, *Science* 334 (2011) 928-9345.
- [5] L. Mai, Q. Wei, Q. An, X. Tian, Y. Zhao, X. Xu, L. Xu, L. Chang, Q. Zhang, *Adv. Mater.* 25 (2013) 2969-2973.
- [6] F. Cheng, J. Liang, Z. Tao, J. Chen, *Adv. Mater.* 23 (2011) 1695-1715.
- [7] N. Liu, H. Wu, M.T. McDowell, Y. Yao, C. Wang, Y. Cui, *Nano Lett.* 12 (2012) 3315-3321.
- [8] L. Cui, J. Shen, F. Cheng, Z. Tao, J. Chen, *J. Power Sources* 196 (2011) 2195-2201.
- [9] P. Poizot, S. Laruelle, S. Grugeon, L. Dupont, J.M. Tarascon, *Nature* 407 (2000) 496-499.
- [10] H. Wang, L.-F. Cui, Y. Yang, H. Sanchez Casalongue, J.T. Robinson, Y. Liang, Y. Cui, H. Dai, *J. Am. Chem. Soc.* 132 (2010) 13978-13980.
- [11] X. Xia, J. Tu, Y. Zhang, J. Chen, X. Wang, C. Gu, C. Guan, J. Luo, H. Fan, *Chem. Mater.* 24 (2012) 3793-3799.
- [12] Z. Wang, L. Zhou, X.W.D. Lou, *Adv. Mater.* 24 (2012) 1903-1911.
- [13] C. Yuan, H. Bin Wu, Y. Xie, X.W.D. Lou, *Angew. Chem. Int. Ed.* 53 (2014) 1488-1504.
- [14] J. Cabana, L. Monconduit, D. Larcher, M.R. Palacín, *Adv. Mater.* 22 (2010) E170-E192.
- [15] A.S. Aricò, P. Bruce, B. Scrosati, J.-M. Tarascon, W. Van Schalkwijk, *Nat. Mater.* 4 (2005) 366-377.
- [16] C. Zhu, X. Xia, J. Liu, Z. Fan, D. Chao, H. Zhang, H.J. Fan, *Nano Energy* 4 (2014) 105-112.
- [17] Y. Sun, X. Hu, W. Luo, Y. Huang, *ACS Nano* 5 (2011) 7100-7107.
- [18] Y. Sun, X. Hu, J.C. Yu, Q. Li, W. Luo, L. Yuan, W. Zhang, Y. Huang, *Energy Environ. Sci.* 4 (2011) 2870-2877.
- [19] W. Luo, X. Hu, Y. Sun, Y. Huang, *J. Mater. Chem.* 22 (2012) 8916-8921.
- [20] B. Liu, X. Hu, H. Xu, W. Luo, Y. Sun, Y. Huang, *Sci. Rep.* 4 (2014) 4229-4234.
- [21] A. Reddy, S. Gowda, M. Shaijumon, P. Ajayan, *Adv. Mater.* 24 (2012) 5045-5064.
- [22] C. Cheng, H. Fan, *Nano Today* 7 (2012) 327-343.
- [23] J. Luo, X. Xia, Y. Luo, C. Guan, J. Liu, X. Qi, C.F. Ng, T. Yu, H. Zhang, H.J. Fan, *Adv. Energy Mater.* 3 (2013) 737-743.
- [24] J. Liu, J. Jiang, C. Cheng, H. Li, J. Zhang, H. Gong, H.J. Fan, *Adv. Mater.* 23 (2011) 2076-2081.
- [25] Y. Wang, J. Xu, H. Wu, M. Xu, Z. Peng, G. Zheng, *J. Mater. Chem.* 22 (2012) 21923-21927.
- [26] Y. Luo, J. Luo, J. Jiang, W. Zhou, H. Yang, *Energy Environ. Sci.* 5 (2012) 6559-6566.
- [27] Q. Xiong, J. Tu, X. Xia, X. Zhao, C. Gu, X. Wang, *Nanoscale* 5 (2013) 7906-7912.
- [28] S. Saadat, J. Zhu, D.H. Sim, H.H. Hng, R. Yazami, Q. Yan, *J. Mater. Chem. A* 1 (2013) 8672.
- [29] W. Zhou, C. Cheng, J. Liu, Y. Tay, J. Jiang, J. Zhang, H. Gong, H. Hng, T. Yu, H. Fan, *Adv. Funct. Mater.* 21 (2011) 2439-2445.
- [30] L. Zhang, G. Zhang, H. Bin Wu, L. Yu, X.W.D. Lou, *Adv. Mater.* 25 (2013) 2589-2593.
- [31] G. Gao, L. Yu, H. Bin Wu, X.W.D. Lou, *Small* 10 (2014) 1741-1745.
- [32] S. Li, Y.-F. Dong, D.-D. Wang, W. Chen, L. Huang, C.-W. Shi, L.-Q. Mai, *Front. Phys.* 9 (2013) 303-322.
- [33] W. Xu, K. Zhao, C. Niu, L. Zhang, Z. Cai, C. Han, L. He, T. Shen, M. Yan, L. Qu, L. Mai, *Nano Energy* 8 (2014) 196-204.
- [34] C. Niu, J. Meng, C. Han, K. Zhao, M. Yan, L. Mai, *Nano Lett.* 14 (2014) 2873-2878.
- [35] L. Zhu, Z. Wen, W. Mei, Y. Li, Z. Ye, *J. Phys. Chem. C* 117 (2013) 20465-20473.
- [36] B. Li, Y. Xie, C. Wu, Z. Li, J. Zhang, *Mater. Chem. Phys.* 99 (2006) 479-486.
- [37] F. Ke, L. Huang, G. Wei, L. Xue, J. Li, B. Zhang, S. Chen, X. Fan, S. Sun, *Electrochim. Acta* 54 (2009) 5825-5829.
- [38] F. Wang, W. Tao, M. Zhao, M. Xu, S. Yang, Z. Sun, L. Wang, X. Song, *J. Alloys Compd.* 509 (2011) 9798-9803.
- [39] Y. Sun, X. Hu, W. Luo, F. Xia, Y. Huang, *Adv. Funct. Mater.* 23 (2013) 2436-2444.
- [40] X. Sun, W. Si, X. Liu, J. Deng, L. Xi, L. Liu, C. Yan, O.G. Schmidt, *Nano Energy* 9 (2014) 168-175.

- [41] J. Luo, J. Liu, Z. Zeng, C.F. Ng, L. Ma, H. Zhang, J. Lin, Z. Shen, H.J. Fan, *Nano Lett.* 13 (2013) 6136-6143.
- [42] H. Fei, Z. Peng, L. Li, Y. Yang, W. Lu, E.L.G. Samuel, X. Fan, J.M. Tour, *Nano Res* 7 (2014) 1-9.
- [43] G. Zhou, D. Wang, F. Li, L. Zhang, *Chem. Mater.* 22 (2010) 5306-5313.
- [44] Q. Hao, J. Wang, C. Xu, *J. Mater. Chem. A* 2 (2014) 87-93.
- [45] X. Gu, L. Chen, S. Liu, H. Xu, J. Yang, Y. Qian, *J. Mater. Chem. A* 2 (2014) 3439-3444.
- [46] C.H. Chen, B.J. Hwang, J.S. Do, J.H. Weng, M. Venkateswarlu, M.Y. Cheng, R. Santhanam, K. Ragavendran, J.F. Lee, J.M. Chen, D.G. Liu, *Electrochem. Commun.* 12 (2010) 496-498.
- [47] J. Li, S. Xiong, Y. Liu, Z. Ju, Y. Qian, *ACS Appl. Mater. Interfaces* 5 (2013) 981-988.
- [48] Z. Xing, Z. Ju, J. Yang, H. Xu, Y. Qian, *Nano Res* 5 (2012) 477-485.
- [49] P. Balaya, H. Li, L. Kienle, J. Maier, *Adv. Funct. Mater.* 13 (2003) 621-625.
- [50] D. Su, M. Ford, G. Wang, *Sci. Rep* 2 (2012) 924-930.
- [51] Y. Xiao, C. Hu, M. Cao, *J. Power Sources* 247 (2014) 49-56.
- [52] L. Hu, N. Yan, Q. Chen, P. Zhang, *Chem. A Eur. J* 18 (2012) 8971-8977.
- [53] H. Huang, W. Zhu, X. Tao, Y. Xia, Z. Yu, J. Fang, Y. Gan, W. Zhang, *ACS Appl. Mater. Interfaces* 4 (2012) 5974-5980.
- [54] C.K. Chan, H. Peng, G. Liu, K. McIlwrath, X.F. Zhang, R.A. Huggins, Y. Cui, *Nat. Nanotechnol* 3 (2008) 31-35.



**Jiexi Wang** received his Bachelor's degree in Metallurgical Engineering from Central South University (CSU) in 2010. He is now a PhD candidate in School of Metallurgy and Environment, Central South University supervised by Prof. Xinhai Li. His research focuses on the synthesis and application of nanomaterials and composites for clean energy storage, such as high-power/high-energy lithium ion batteries, and supercapacitors.



**Qiaobao Zhang** obtained his M.S. degree in Electrochemistry from Xiamen University in 2010. He is now pursuing his PhD degree at Department of Mechanical and Biomedical Engineering, City University of Hong Kong. His research focuses on the synthesis and application of novel metal oxide nanostructures and their composites for energy storage, including lithium ion batteries and supercapacitors.



**Xinhai Li** received his Ph.D in physical chemistry from Central South University of Technology in 1990. Currently he is a Professor and Director of the Engineering Center for Advanced Materials for Energy Storage in School of Metallurgy and Environment, CSU. He is an expert in energy database of China. He mainly works on carbon materials, materials for batteries and supercapacitors, design and application of energy storage and conversion systems,

electrolyte for lithium ion batteries, and resource-to-material metallurgy. His research works have been published in *Journal of Materials Chemistry*, *Chemical Communications*, *Nano Energy*,

*Nanoscale*, *Electrochemistry Communications*, *Journal of Power Sources*, *The Journal of Physical Chemistry C*, *Electrochimica Acta*, etc.



**Bao Zhang** received his Ph.D. degree from Central South University in 2005. He is now a professor of materials physical chemistry in the School of Metallurgy and Environment, CSU. His main research interests include phosphate-based materials and heterostructured materials for lithium storage, EV cell, extractive metallurgy. His research works have been published in *Chemical Communications*, *ACS Applied Materials & Interface*, *Journal of Power Sources*, *Electrochimica Acta*, etc.



**Liqiang Mai** received his Ph.D. degree from Wuhan University of Technology in 2004. He then carried out postdoctoral research in the laboratory of Professor Zhonglin Wang at Georgia Institute of Technology in 2006-2007 and worked as an advanced research scholar in the laboratory of Professor Charles M. Lieber at Harvard University in 2008-2011. He is Chair Professor of Materials Science and Engineering at Wuhan University of Technology and Executive Director of the WUT-Harvard Joint Nano Key Laboratory. He has published more than 110 papers tagged by SCI in peer-reviewed journals such as *Nature Nanotechnology*, *Nature Communications*, *Chemical Reviews*, *Proceedings of the National Academy of Sciences*, *Journal of the American Chemical Society*, *Nano Letters*, *Advanced Materials*, and so forth. His interests include nanowire materials, micro/nanoenergy storage devices, and energy-based nano-bio interface.



**Kaili Zhang** received his PhD degree from National University of Singapore in 2006. He then worked as postdoctoral researchers at French National Center for Scientific Research (LAAS-CNRS) and Swiss Federal Institute of Technology Zurich (ETH Zurich). He is now working as an assistant professor at Department of Mechanical and Biomedical Engineering, City University of Hong Kong. His research interests include nanomaterials for energy storage applications, energetic materials, and nanoenergetics-on-a-chip. His research results have been published in *Progress in Materials Science*, *Nano Energy*, *Small*, *ChemSusChem*, *Nano Research*, *Combustion and Flame*, *Energy*, *Applied Energy*, etc. with a total citation > 1200 (h-index=18).